

# Rethinking Image-Scaling Attacks: The Interplay Between Vulnerabilities in Machine Learning Systems

Yue Gao  
gy@cs.wisc.edu  
University of Wisconsin–Madison

Ilia Shumailov  
ilia.shumailov@cl.cam.ac.uk  
University of Cambridge

Kassem Fawaz  
kfawaz@wisc.edu  
University of Wisconsin–Madison

## Abstract

As real-world images come in varying sizes, the machine learning model is part of a larger system that includes an upstream image scaling algorithm. In this system, the model and the scaling algorithm have become attractive targets for numerous attacks, such as adversarial examples and the recent image-scaling attack. In response to these attacks, researchers have developed defense approaches that are tailored to attacks at each processing stage. As these defenses are developed in isolation, their underlying assumptions may not hold when viewing them from the perspective of an end-to-end machine learning system. Thus, it is necessary to study these attacks and defenses in the context of machine learning systems.

In this paper, we investigate the interplay between vulnerabilities of the image scaling procedure and machine learning models in the challenging hard-label black-box setting. We propose a series of novel techniques to make a black-box attack exploit vulnerabilities in scaling algorithms, scaling defenses, and the final machine learning model in an end-to-end manner. Based on this scaling-aware attack, we reveal that most existing scaling defenses are ineffective under threat from downstream models. Moreover, we empirically observe that standard black-box attacks can significantly improve their performance by exploiting the vulnerable scaling procedure. We further demonstrate this problem on a commercial Image Analysis API with transfer-based black-box attacks.

## 1 Introduction

Recent advances in machine learning (ML) techniques have demonstrated human-level performance in many vision tasks, such as image classification [40, 44, 45] and object detection [38, 39]. As real-world images come in varying sizes, the ML system includes an image scaling algorithm followed by a downstream ML model. The scaling algorithm resizes input images to match the fixed input size of a model, which takes the input and performs vision tasks, such as classification.

The model and scaling algorithm in an ML system have become attractive targets for attackers. ML models are known as vulnerable to adversarial examples [6, 46]; an adversary can add imperceptible perturbations to the input of a model and change its prediction [10, 32]. Such attacks can take place in the white-box setting where the attacker has access to the model parameters or the black-box setting where the attacker only has access to model outputs or a surrogate model. Recently, scaling algorithms in the ML system were shown as vulnerable to image-scaling attacks [35, 48]; an adversary can manipulate a source image

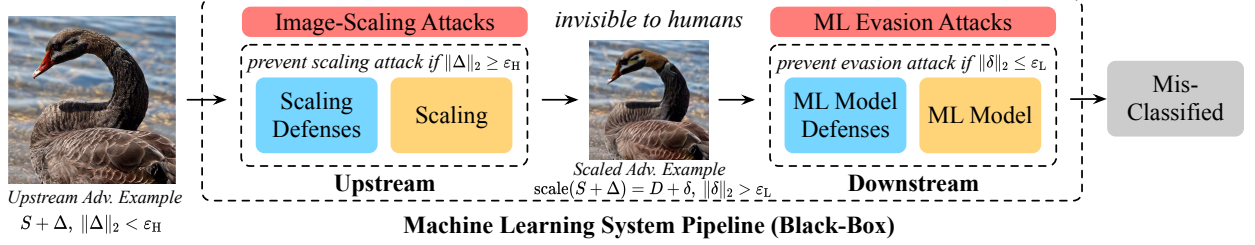


Figure 1: Illustration of the real-world machine learning system pipeline under different attacks. The scaling defenses [29, 35] protect against attackers injecting a clean image (i.e.,  $\Delta$  is large) into the source image  $S$ . The ML defenses [32] are designed to be robust against imperceptible adversarial perturbation (i.e.,  $\delta$  is small). Both defenses are effective under their respective assumptions. We showcase a new perspective where a black-box adversary can circumvent both defense strategies by jointly exploiting vulnerabilities. Effectively, the user would consider the overall system as vulnerable to imperceptible perturbations, although the standalone model is not.

such that it will change into a different target image after scaling, thereby inducing an incorrect prediction in the downstream classifier.

In response to these attacks, researchers have developed defense approaches tailored to each processing stage. Figure 1 illustrates an overview of such attacks and defenses in an ML system pipeline. First, several scaling defenses [29, 35] have effectively mitigated the image-scaling attack. These defenses, similar to the scaling attacks, assume the injected target image to be sufficiently different from the source image. Second, robust ML defenses, such as adversarial training [8, 32], defend against adversarial examples of norms below a preconfigured perturbation budget. As these defenses are developed in isolation, their underlying assumptions may not hold when viewing them from the perspective of an ML system.

To attack the ML system, the adversary manipulates an input image to induce a misclassification. The scaling defense, with the underlying assumption of injecting a sufficiently different image, does not fare well if the adversary jointly targets the downstream ML model. For example, the adversary can incorporate adversarial perturbations smaller than the magnitude that the defense was designed to handle. Similarly, the ML defense, which claims robustness against adversarial examples within a certain perturbation budget, can be ineffective if the adversary jointly targets the upstream scaling algorithm. For example, the adversary can leverage weaknesses in image scaling to produce an attack image that satisfies the perturbation budget before scaling, but violates it afterward. Because the scaling procedure and the violation of perturbation budgets both occur inside the system, they are opaque to the users.

As such, it is necessary to study these attacks and defenses in the context of the ML system pipeline. Such a study informs the effectiveness of cutting-edge defenses for scaling and ML models when the adversary targets the entire ML system. In this paper, we investigate the interplay between the vulnerabilities in an ML system, including those of the scaling algorithms and the ML models.

As a first step, we provide theoretical intuition to analyze how the vulnerability in ML models impacts scaling defenses. Then, we show how a black-box attack can jointly exploit the vulnerability of scaling and ML models. In order to evaluate scaling defenses within their original threat model, we base our study on a recently proposed hard-label black-box attack, i.e., the HopSkipJump (HSJ) [13] attack. Similar to image-scaling attacks, the HSJ attack sends queries to the ML system and receives only the final decision without confidence scores. We propose a series of novel techniques to make the HSJ attack aware of scaling algorithms, scaling defenses, and the final ML model. As a result, the scaling-aware HSJ attack effectively

targets the entire ML system in an end-to-end manner. We also provide scaling-aware white-box attacks such as PGD [32] and C&W [10] to enable transfer-based attacks and worst-case evaluation of existing scaling defenses.

We conduct a comprehensive evaluation to study the interplay between vulnerabilities based on our scaling-aware attacks. Our evaluation reveals three main findings.

- In the black-box setting, our scaling-aware HSJ attack successfully leverages the weakness in scaling algorithms (even under defenses) to significantly improve the performance of the vanilla HSJ attack. For the same query budget, scaling-aware attacks are able to generate less perturbed adversarial examples than vanilla attacks.
- In both the black-box and white-box settings, we show that scaling-aware attacks can evade four out of five state-of-the-art scaling defenses. These defenses include the median filtering defense [35] and three detection defenses [29]. However, we find that randomized filtering defense [35] is effective under our attack even in the white-box setting. Further, we provide a theoretical argument to explain the effectiveness of these defenses.
- Finally, we show that scaling-aware white-box attacks perform significantly better than vanilla attacks. For the same perturbation budget, they generate stronger and more confident adversarial examples. We further show how an adversary can attack a surrogate model to generate less perturbed adversarial examples that transfer to a commercial Image Analysis API.

Furthermore, our work provides an interesting insight into the field of ML security research. While an attacker may choose to exploit only one vulnerability in the ML system, defenders should be cautious when depending on the same assumption as the attacker, especially if this assumption depends on the security of other components in the system. For example, the clean-image assumption that empowers the image-scaling attack turns out to disqualify its defenses.

## 2 Background and Related Work

In this paper, we study attacks and defenses through an end-to-end view of the ML system. Previous research has investigated components in the ML system, such as the image-scaling attacks [14, 35, 36, 48] and defenses [29, 35, 36], as well as the ML model attacks [10, 13, 26, 32] and defenses [8, 18, 27, 32]. Our work extends existing research by introducing a novel perspective of the whole ML system pipeline along with a case study of the scaling procedure. We provide comprehensive analysis and evaluation of image-scaling defenses and ML model attacks to show that different vulnerabilities in an ML system can exacerbate each other. This whole-system view further motivates an extensive evaluation of current ML system’s robustness [12, 23, 42, 43]. For example, audio systems usually have a complicated pipeline that may introduce unexplored vulnerabilities [47], and facial recognition systems are already vulnerable to transfer-based attacks [11, 17, 24, 41] that are potentially improvable due to the scaling vulnerability.

In the following, we briefly review the background necessary to understand the ML system pipeline, as well as the attacks and defenses for scaling algorithms and ML models.

## 2.1 Machine Learning System Pipeline

ML models designed for vision tasks accept image inputs of a fixed size. For example, the widely used model ResNet [28] accepts  $224 \times 224$  input images<sup>1</sup>. As real-world ML systems must cater for input images of varying sizes, the ML pipeline must include an image scaling component, as demonstrated in Figure 1. The end-to-end ML pipeline accepts an input image  $S$  of high resolution. It includes a scaling stage that downscales  $S$  to  $D$  in low resolution, which matches the input dimensions of the ML model. The ML model takes image  $D$  as an input and predicts a corresponding label; we mainly focus on downstream models that perform classification. As the background for ML models is well-documented in the literature, we review the less-explored scaling procedure below.

**Image Scaling.** The scaling procedure,  $\text{scale}(\cdot)$ , resizes a high-resolution (HR) source image  $S \in \mathbb{R}^{m \times n}$  to the low-resolution (LR) output image  $D \in \mathbb{R}^{p \times q}$ . The overall scaling ratio is defined as  $\beta = \min\{\beta_h, \beta_v\}$ , where  $\beta_h = n/q$  and  $\beta_v = m/p$  are the scaling ratios in two directions. In this paper, we only consider downscaling where  $\beta > 1$ . The scaling function can be implemented in different ways; we review two formulations that facilitate our analysis.

**Matrix Multiplication.** Xiao et al. [48] conduct an empirical analysis of common scaling functions. They propose to represent image scaling as matrix multiplications:

$$D = \text{scale}(S) = L \times S \times R, \quad (1)$$

where  $L \in \mathbb{R}^{p \times m}$  and  $R \in \mathbb{R}^{n \times q}$  are the two constant coefficient matrices determined by the applied scaling function. They also provide an efficient strategy to deduce approximations of these matrices from given implementations.

**Convolution.** Quiring et al. [35] interpret scaling as a convolution<sup>2</sup> between the source image  $S$  and a fixed linear kernel  $k$  determined by the scaling algorithm:

$$D = \text{scale}(S) = S \star k, \quad (2)$$

where  $\star$  denotes the 2D convolution with proper padding and stride size to match the desired output shape.

## 2.2 Image-Scaling Attacks

The scaling attack targets the scaling procedure in an ML system pipeline. Xiao et al. [48] and Quiring et al. [35] have demonstrated that an attacker can exploit the scaling procedure to compromise an arbitrary downstream ML model. Figure 2 illustrates the pipeline of this attack. An adversary computes the attack image  $A$  by adding imperceptible perturbations  $\Delta$  to the source image  $S$ , such that it becomes similar to a target image  $T$  (with a different label from  $S$ ) after scaling, thereby fooling the downstream classifier. They formulate the scaling attack as a quadratic optimization problem:

$$\min \|\Delta\|_2^2 \quad \text{s.t.} \quad \|\text{scale}(S + \Delta) - T\|_\infty \leq \epsilon, \quad (3)$$

where the attack image  $A := S + \Delta$  satisfies the box constraint  $A \in [0, 1]^{m \times n}$ .

Besides empirical attacks, Quiring et al. [35] conduct an in-depth analysis of common scaling algorithms and corresponding convolution kernels used in Equation (2). They identify the use of non-uniform kernels

<sup>1</sup>We will omit the channel dimension in the rest of this paper.

<sup>2</sup>More precisely, this should be cross-correlation [19]. But we will use the term convolution for consistency.

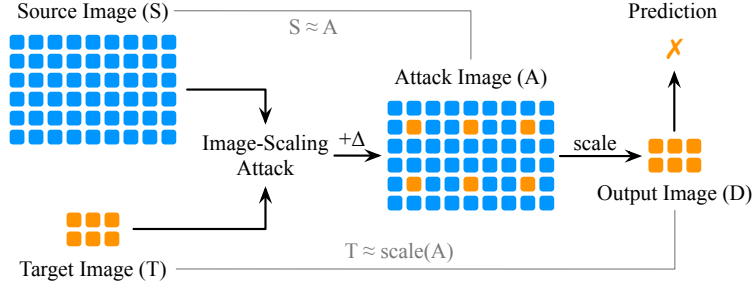


Figure 2: Illustration of the image-scaling attack pipeline. The adversary computes the attack image  $A$  such that it looks similar to the source image  $S$ , but becomes similar to a target image  $T$ . The color indicates pixels from different images.

of a fixed width as the root cause for scaling attacks. Such kernels assign higher weights to a small set of *vulnerable pixels* in the source image. For example, in Figure 2, the attacker only needs to modify a few vulnerable (orange) pixels in the source image to change the scaling output completely.

The scaling attack works under the black-box threat model. It only needs hundreds of decision-only queries to deduce the fixed scaling algorithm in an ML system [48].

## 2.3 Image-Scaling Defenses

Researchers proposed several add-on defenses against the scaling attack; these defenses fall into two categories: prevention and detection defenses. We review five state-of-the-art defenses as summarized in Table 1.

### 2.3.1 Prevention Defenses

Quiring et al. [35] propose the only two prevention defenses, i.e., median and randomized filtering. Both defenses apply filtering operations to sanitize the input image before scaling. Specifically, they reconstruct each vulnerable pixel by a median or a randomly picked pixel within a sliding window. As a result, the attacker has to perturb a significantly larger number of pixels within a window to evade these defenses. Finally, Quiring et al. claim that the median filtering defense is more practical; the randomized filtering defense could hurt the downstream classifier’s performance [35]. We analyze these defenses with more details in Sections 3.2 and 3.3

Defense	Type	Technique
Median [35]	Prevention	Apply median filtering in a window.
Randomized [35]	Prevention	Randomly sample pixels in a window.
Unscaling [29]	Detection	Apply down- and up-scaling to detect perturbation.
Min-filtering [29]	Detection	Apply min-filtering to reveal injected perturbation.
Spectrum [29]	Detection	Identify peaks in the centered spectrum.

Table 1: Techniques used by recent scaling defenses.

### 2.3.2 Detection Defenses

Kim et al. [29] propose three detection defenses using spatial and frequency transformations: unscaling, minimum-filtering, and centered spectrum. These transformations result in discernible differences when applied to benign and attack images. The unscaling invokes downscale and upscale operations sequentially to reveal the injected image. If the input image is benign, this procedure should reveal a similar image to the original input one. In case of an attack image, this sequence would reveal a different image. Similarly, minimum-filtering reveals such differences using the minimum filter operation. By measuring this difference, they construct a threshold-based detector using mean squared error (MSE) and structural similarity index (SSIM). They also notice that the attack perturbation manifests as high-energy and high-frequency noise, which is detectable by examining the spectrum image. We analyze these defenses with more details in Section 3.4.

### 2.3.3 Robust Scaling Algorithms

Besides the above add-on defenses, Quiring et al. [35] identify several scaling algorithms that are naturally robust to the scaling attack. These algorithms are robust because they use either uniform kernels or dynamic kernel widths. For instance, the area scaling algorithm convolves the input image (of scaling ratio  $\beta$ ) with a uniform kernel  $k_{\text{area}}$  of size  $\beta \times \beta$ , where each entry of  $k_{\text{area}}$  is set to  $1/\beta^2$  – the kernel considers each pixel in the window equally. Thus, the attacker cannot find vulnerable pixels to inject another image stealthily.

Ideally, such algorithms should be part of the ML pipeline, but the default scaling algorithm in common ML frameworks is not robust [35]. Thus, switching to a different (robust) algorithm faces compatibility issues, such as changing dependent libraries, performance degradation, and even model retraining. As such, deployed ML systems would prefer add-on defenses that can easily fit as plugin modules [29]. However, our analysis in Section 3 shows that ML systems need to avoid such add-on defenses; they should deploy scaling algorithms that are robust by design.

## 2.4 ML Model Attacks

The ML model is known as vulnerable to numerous attacks. Here, we only consider untargeted evasion attacks that aim to induce a misclassification with minimum  $\ell_2$ -norm perturbation to an input. Such attacks can take place in both black-box and white-box settings.

### 2.4.1 Black-box Evasion Attacks

In this setting, the attacker does not have knowledge of the model parameters. But, the attacker can send hard-label (decision) or soft-label (prediction score) queries to the model. As queries come with monetary costs, the attacker’s main objective is to minimize the perturbation as well as the number of queries. To stay consistent with the setting under which the image-scaling attack was developed, we only consider the more challenging hard-label setting.

Most hard-label attacks choose to walk near the decision boundary, such as the Boundary attack [7] and the recent HopSkipJump [13] attack. These attacks employ an iterative algorithm to solve the following optimization problem:

$$\min_{\mathbf{x}'} \|\mathbf{x}' - \mathbf{x}\|_2 \quad \text{s.t. } \mathbf{x}' \text{ is misclassified.} \quad (4)$$

The iterative algorithm can be summarized in three steps: (1) Find a point  $\mathbf{x}'$  near the decision boundary through a linear search starting from  $\mathbf{x}$ ; (2) Sample noise around  $\mathbf{x}'$  to estimate the gradient; (3) Use the

gradient to update  $\mathbf{x}'$ . This algorithm finds an adversarial example at the first step but requires more iterations to decrease the perturbation size. Other hard-label black-box attacks are primarily based on optimization techniques [15, 16] or geometry properties [31, 37].

### 2.4.2 White-box Evasion Attacks

In this setting, the attacker has full knowledge of the model parameters. The attacker’s main objective thus becomes minimizing the adversarial perturbation. Examples of powerful white-box attacks are the C&W [10] and Projected Gradient Descent (PGD) [32].

The C&W [10] attack finds the minimal adversarial perturbation  $\delta$  for an input image  $\mathbf{x}$  by solving the following optimization problem:

$$\min_{\delta} \|\delta\|_2 + c \cdot f(\mathbf{x} + \delta; \kappa) \quad \text{s.t. } \mathbf{x} + \delta \in [0, 1]^n, \quad (5)$$

where  $c$  is a constant determined by a binary search procedure and  $f$  is a loss function quantifying the confidence of a ground-truth prediction. A hyper-parameter  $\kappa$  controls the confidence of produced adversarial examples.

The PGD [32] attack employs an iterative algorithm to solve the following constrained optimization problem:

$$\max_{\delta} J(\text{model}(\mathbf{x} + \delta), y) \quad \text{s.t. } \|\delta\|_2 \leq \epsilon, \quad (6)$$

where  $\epsilon$  upper-bounds the adversarial perturbation in  $\ell_2$ -norm,  $y$  is the ground truth label, and  $J$  is the cross entropy loss. This attack is commonly used to assess the model’s robustness under certain perturbation budgets.

## 2.5 ML Model Evasion Defenses

While there are numerous defenses against ML evasion attacks, adversarial training [32] remains as one of the most effective empirical defenses [8]. It views adversarial examples (generated during training) as worst-case examples and includes them in the training data. It serves as a strong baseline to assess evasion attacks in the white-box setting.

## 3 Scaling Defense Analysis

We start by investigating how the vulnerability in ML models impacts the vulnerability in scaling algorithms and defenses.

Note that existing scaling defenses, thus far, only considered attackers feeding the downstream model a clean image (without adversarial perturbation) to change its prediction; we refer to this as the “clean-image” assumption. While this assumption is obviously advantageous for a scaling *attack*, we note that a scaling *defense* should be cautious when leveraging the same assumption. This assumption does not hold when we consider the vulnerability in downstream models. For example, Quiring et al. [36] violate this assumption by poisoning the downstream model and observe that most previous detection defenses are ineffective. However, their attack requires control of the model’s training process, which may not be realistic for most of the attackers.

In contrast, we examine scaling defenses under the more constrained black-box setting, as we will discuss later in Section 4.1. Our intention is to understand if defenders should consider the interplay between



different vulnerabilities while building a defense. In the case of scaling defenses, we want to know if they implicitly rely on the clean-image assumption and how effective they are when this assumption is violated. Therefore, we conduct an in-depth analysis of the mechanism behind existing scaling defenses. We conclude that ML systems need to avoid these add-on defenses; they should deploy scaling algorithms that are robust by design.

### 3.1 Effective Scaling Defenses

Before analyzing a specific scaling defense, we discuss what it means for a scaling defense to be effective (or robust under the terminology from Quiring et al. [35]). Prevention defenses are effective if images do not change their appearance after the defended scaling, such that the attacker cannot hide a large perturbation stealthily. Since a defended scaling procedure can be viewed as a new scaling function, we note that it must also satisfy the argument from Quiring et al. [35] about robust scaling algorithms (refer Section 2.3.3). This simple observation indicates that an effective prevention defense should process the input, such that the followed scaling function can weight all pixels uniformly. As for detection defenses, they are effective if they can detect the attack with acceptable false acceptance and rejection rates.

### 3.2 Median Filtering

The median filtering defense sanitizes the input image by sliding a window  $w$  around vulnerable pixels and applying the median filter  $f_{\text{med}}$ . To evade this defense, an adaptive attacker has to perturb pixels in each window  $w$ , such that the filtering output  $w_m = f_{\text{med}}(w)$  changes to a desired value  $w_t$ .

Quiring et al. [35] regard this defense as robust to an adaptive attacker that changes the filter’s output by setting pixels within range  $R := [w_m, w_t]$  to  $w_t$ . However, this defense fails to satisfy the robustness requirement of uniform weights. Since  $|R| \leq |w|/2$ , the attacker needs only to modify at most half of the pixels to change the filtering output into a target value.

The above observation further implies that the effectiveness of median filtering defense relies on the (large) value of  $|R|$ . In its original evaluation,  $|R|$  is always large due to the clean-image assumption. However, in case of an adversarial example, the target pixel  $w_t$  will be close to the original output  $w_m$ , implying a small range  $R = [w_m, w_t]$  that decreases the effectiveness. Thus, the median filtering defense is only effective when the clean-image assumption holds.

### 3.3 Randomized Filtering

The randomized filtering defense sanitizes the input image by sliding a window  $w$  around vulnerable pixels and applying the random filter  $f_{\text{rnd}}$ , which randomly picks a pixel from  $w$ . To evade this defense completely, an adaptive attacker has to set every pixel in a window to the desired value.

Quiring et al. [35] regard this defense as robust but associate it with a minor degradation in model performance [35]. Interestingly, this less-recommended defense meets the requirement of robust scaling. Specifically, we find that the expectation (over the randomized filter) of randomized filtering defense can be viewed as an area scaling procedure:

$$\mathbb{E}_{\text{defense} \sim \mathcal{D}}[(\text{scale} \circ \text{defense})(S)] = S \star \mathbf{k}_{\text{area}}, \quad (7)$$

where  $\mathcal{D}$  is the space of defense functions chosen by the randomized filtering defense and  $\mathbf{k}_{\text{area}}$  is the uniform area scaling kernel (refer to Section 2.3.3). A theoretical argument can be found in Appendix A. This observation shows that the randomized filter can process the input such that any followed scaling



function becomes uniform in expectation. Thus, we conclude that the randomized filtering defense is still effective, even when the clean-image assumption does not hold.

### 3.4 Detection Defenses

Detection defenses aim to detect the perturbation injected by scaling attacks. A detector determines whether the input image  $x \in \{S, A\}$  is benign ( $S$ ) or perturbed by the scaling attack ( $A := S + \Delta$ ). Here, we study the detection defenses from Kim et al. [29], as summarized in Table 1.

In the spatial domain, both the unscaling and min-filtering methods reveal the injected perturbation through processing the input image  $x$  with some function  $h$ . For example, the unscaling defense considers  $h$  as the composition of downscaling and upscaling. After that, they quantify the resulting distortion with perceptual metrics like MSE and SSIM. For instance, one could model the distortion score as  $t(x) := \text{MSE}(x - h(x))$  and employ a threshold-based detector to determine whether the input image  $x$  is benign or perturbed.

In the frequency domain, the spectrum defense examines the number of peaks in the spectrum image, as it assumes injected perturbations manifest as high-frequency and high-energy noise. It applies a low-pass filter (with a predefined threshold) on the input’s spectrum image to reveal such peaks.

Overall, these detection defenses rely on a threshold-based mechanism, but this threshold is only easy to find under the clean-image assumption. When this assumption does not hold, there may not exist a threshold to allow for acceptable false acceptance and rejection rates.

## 4 Scaling-aware Black-Box Attacks

Our analysis in Section 3 requires an attacker that exploits both the scaling procedure and ML models in the black-box setting. In this section, we instantiate this attacker by making black-box attacks aware of the upstream scaling procedure as well as scaling defenses. However, designing a scaling-aware black-box attack is challenging as it requires exploiting weaknesses inside a black-box system. To overcome this challenge, we propose a series of novel techniques to enable a scaling-aware attack pipeline that targets the entire ML system. We demonstrate this pipeline with a case study of a recently proposed hard-label black-box attack.

Our construction of a scaling-aware attack contributes to the understanding of how vulnerability in scaling cascades through the pipeline and ultimately makes ML models vulnerable. We observe an inconsistency when evaluating the robustness of an ML model from the perspective of the ML system pipeline. A standalone ML model may be robust to evasion attacks within certain  $\ell_2$ -norm budgets; this claim establishes an expectation that the ML model is only vulnerable to perceptible perturbations (i.e., those with norms larger than the specific  $\ell_2$ -norm budget). However, the adversary can exploit the scaling vulnerability to obtain an upstream adversarial perturbation that is imperceptible before scaling but violates the  $\ell_2$ -norm budget after scaling. Because the scaling procedure and the violation of perturbation budget both occur inside the system, they are opaque to the users – the user need not be concerned with the perceptible perturbation after downscaling. The user will regard the ML model as not robust, although the actual robustness of this standalone model remains valid.

### 4.1 Threat Model

We focus on the hard-label black-box setting where the attacker can only send queries to the ML system and receive the final decision. This setting is consistent with the image-scaling attack, which requires hundreds

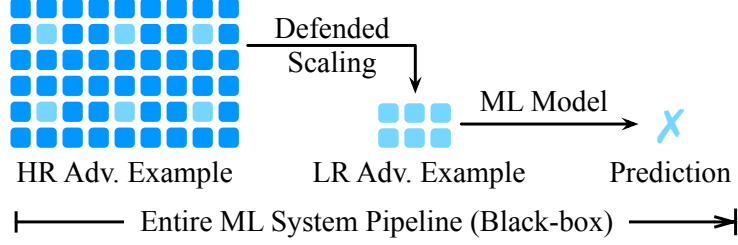


Figure 3: Scaling-aware attack targets at the entire ML system as a black-box. Light blue indicates pixels of imperceptible adversarial perturbations of the downstream ML model.

of hard-label queries to deduce the scaling algorithm in an ML system [48]. To stay consistent with previous work studying black-box attacks [7, 13, 15, 16], the victim ML model does not deploy any defenses like adversarial training. For the purpose of evaluation, we also consider transfer-based black-box attacks with access to a surrogate model, and white-box attacks with full knowledge of the model parameters. In the white-box setting, we protect the victim ML model with adversarial training to allow for an informative evaluation. We only consider untargeted attacks for simplicity. Although targeted attacks typically require a larger perturbation, such perturbation is still much smaller than a different image and thus shares the same insights as untargeted attacks.

In all settings, we assume the targeted ML system includes a scaling procedure, a potential prevention scaling defense, and the final ML model. We assume the knowledge of scaling defenses like previous works [29, 35]. However, we note that it is possible to deduce such knowledge by enumerating all the defenses, as there is only a limited set of them.

## 4.2 Attack Pipeline

Making black-box attacks aware of scaling requires incorporating the scaling algorithm, scaling defenses, and the ML model in one attack pipeline, as illustrated in Figure 3. While this is similar to deploying vanilla black-box attacks on the complete ML pipeline that accepts high-resolution images, that approach will not be able to leverage the vulnerability of scaling algorithms; it would provide a false sense of security about the security properties of the overall model. In the following, we provide a case study on one of the most powerful black-box attacks to demonstrate how to make existing black-box attacks aware of scaling.

**Case Study: HopSkipJump (HSJ).** The HSJ attack is a hard-label black-box attack, which sends queries to acquire the final decision instead of the probability or confidence score. It uses an iterative algorithm (refer to Section 2.4.1) to walk near the decision boundary while minimizing the perturbation.

We incorporate scaling by modifying HSJ’s iterative algorithm. Specifically, we encode this knowledge in the *noise sampling* procedure that estimates the gradient information. The modified HSJ attack can be summarized in three steps: (1) Find a point  $x'$  near the decision boundary through a line search from the input  $x$  along a given direction; (2) Sample noise around  $x'$  that *incorporates the knowledge of scaling* to estimate the gradient at the decision boundary; (3) Use the gradient to update the direction to search for a new  $x'$ .

However, encoding such knowledge is not straightforward. While the scaling procedure is conceptually similar to a preprocessing defense, we are unable to use the white-box technique BPDA [3] because there is no backward pass through the network in black-box attacks. To overcome this problem, we propose several novel techniques to help incorporate scaling. Algorithm 1 shows the final modified algorithm. We

---

**Algorithm 1** Scaling-aware HSJ Attack (Simplified)

---

**Require:** Scaling procedure  $\text{scale}(\cdot)$ , classifier  $C$ , an image  $x$ , iterations  $T$ , other parameters for HSJ attack.

**Ensure:** Perturbed image  $x_t$ .

Initialize  $\tilde{x}_0$  such that  $C(\tilde{x}_0) \neq C(x)$ .

**for**  $t$  in  $1, 2, \dots, T$  **do**

▷ Binary Search

Find  $x_t$  near the boundary between  $x$  and  $\tilde{x}_{t-1}$ .

▷ **Scaling-aware Noise Sampling (Section 4.3)**

Sample unit vectors  $\{u_1, u_2, \dots\}$  using Equation (9).

▷ Gradient-direction Estimation

Estimate gradient direction  $g$  with  $\{u_1, u_2, \dots\}$ .

▷ Update Perturbed Image

Search the step size  $\xi$ .

Set  $\tilde{x}_t \leftarrow x_t + \xi \cdot g$ .

**end for**

Find  $x_t$  near the boundary between  $x$  and  $\tilde{x}_{t-1}$ .

Output  $x_t$ .

---

refer readers to the original HSJ attack [13] for more details about the HSJ attack (HSJA). Final adversarial examples produced by scaling-aware HSJA are shown in Figure 4; they obtain less perturbation than the vanilla HSJA. We provide more examples in Appendix E.

We note that we only consider the median filtering defense, because we have analyzed the effectiveness of randomized filtering in Section 3.3 with an empirical verification in the white-box setting in Section 6.5. We also empirically find that the modified attack evades all existing detection defenses out of the box. Lastly, we discuss a less effective approach that sequentially exploits the scaling procedure and ML models in Appendix B. That approach returns suboptimal results not guaranteed to be adversarial, as we evaluate in Section 6.3.

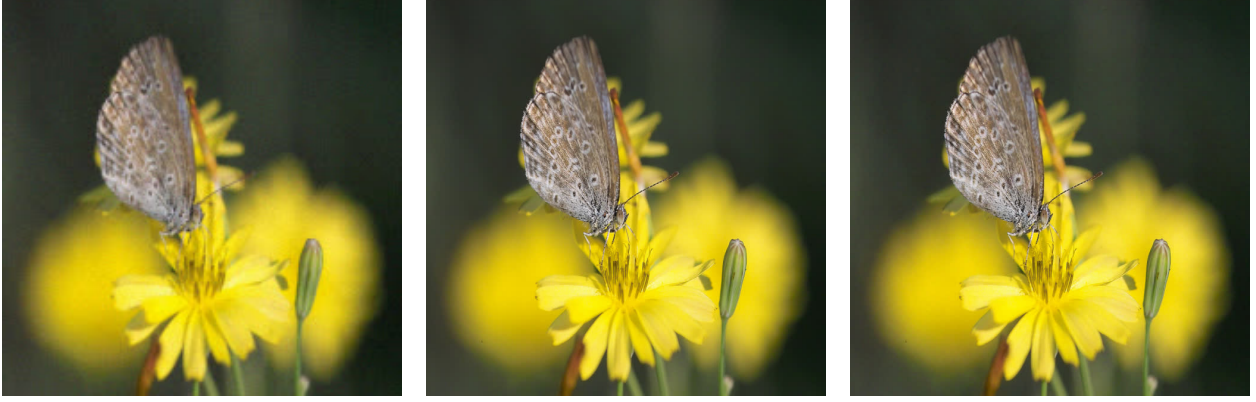
### 4.3 Incorporating Scaling

We start by showing how to incorporate scaling algorithms. The matrix multiplication formulation of scaling from Xiao et al. [48] (refer to Section 2.1) indicates that the scaling procedure can be viewed as a linear mapping from the high-resolution (HR) space to a low-resolution (LR) subspace. Since a vanilla attacker estimates the gradient using noise sampled in the HR space, they cannot exploit vulnerabilities in scaling when mapping to the LR space. To overcome this challenge, we propose a novel technique called *Scaling-aware Noise Sampling* to sample HR noise that lies on the LR subspace, as illustrated in Figure 5.

#### 4.3.1 Scaling-aware Noise Sampling (SNS)

The proposed scaling-aware noise sampling consists of two steps: (1) sample noise  $u'$  in the LR subspace; and (2) project the LR noise  $u'$  back to the HR space. Figure 5 illustrates this novel sampling procedure. The first step is straightforward as the LR subspace is well-defined by the scaling procedure. As for the second step, a straightforward approach is to compute the exact projection by solving an optimization problem:

$$u^* := \arg \min_u \|\text{scale}(x + u) - (\text{scale}(x) + u')\|_2, \quad (8)$$



(a) HSJA-Vanilla (scaled  $\ell_2 = 5.89$ ) (b) HSJA-Scaling (scaled  $\ell_2 = 2.03$ ) (c) HSJA-Median (scaled  $\ell_2 = 2.36$ )

Figure 4: Adversarial examples from (a) HSJA, (b) scaling-aware HSJA, and (c) scaling-aware HSJA under the median filtering defense. The query budget is set to 5K. The original shape is  $224 \times 224$  for (a), and  $672 \times 672$  for (b) and (c). Scaling-aware HSJA produces less perturbation even under the median filtering defense.

where  $\mathbf{u}^*$  is the HR noise that lies on the LR subspace.

However, this approach is computationally prohibitive, as we need to solve an optimization problem for every single noise sampling. We overcome this problem by proposing the efficient version of SNS.

#### 4.3.2 Efficient SNS

Recall that the objective of SNS is only to find an HR *noise* sample that lies on the LR subspace. Thus, there is no need to find the *exact* projection of a *random* noise sample. Based on this observation, we note that an *imprecise projection* suffices to estimate the gradient. One efficient imprecise projection we found is the gradient of Equation (8), written as

$$\mathbf{u}^* := \nabla_{\mathbf{u}} \|\text{scale}(\mathbf{x} + \mathbf{u}) - (\text{scale}(\mathbf{x}) + \mathbf{u}')\|_2. \quad (9)$$

Finally, we use the more efficient Equation (9) to sample noise  $\mathbf{u}^*$ , in the HR space, that lies on the LR subspace. Afterward, we follow the same procedure as vanilla HSJ attack, which takes a set of the noise samples  $\mathbf{u}^*$  to estimate the gradient direction and searches for a new  $\mathbf{x}'$  along this direction near the decision boundary, as illustrated in Algorithm 1.

#### 4.4 Incorporating Median Filtering

The next step is to incorporate median filtering defense. While our proposed SNS is compatible with the projection defined by median filtering as well, we find that the gradient of standard median function is inefficient in the black-box setting and significantly slows down the HSJ attack’s convergence. To overcome this problem, we propose a *gradient-efficient* approximation of the median filtering when computing its projection in SNS through Equation (9).

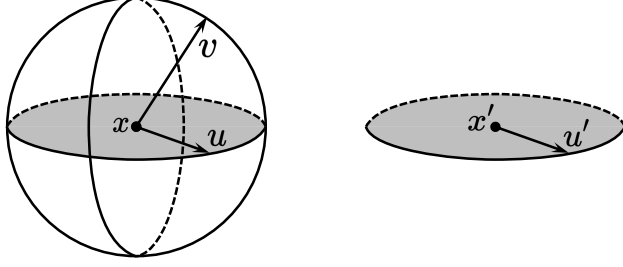


Figure 5: Scaling-aware noise sampling (SNS). In the HR space (left), randomly sampled noise  $v$  is unlikely to find the exploitable subspace (grey). SNS overcomes this problem by first sampling noise  $u'$  in the LR space (right) and then projecting it back to the HR  $u$ , which lies on the LR subspace.

#### 4.4.1 Inefficiency of Standard Median

To emphasize why the gradient of standard median is inefficient in the black-box setting, we illustrate how the HSJ attack conducts line search along a direction estimated from noise samples in Equation (9). Consider an example  $x = [1, 3, 2]$ , which results in a noise sample  $u^* = [0, 0, 1]$  due to Equation (9) and its corresponding direction  $g = u^*$ . Because all non-median directions are zero, only the last entry in  $u^*$  is non-zero. In this case, the line search procedure simply attempts  $\{x + g, x + 2g, \dots\}$  until reaching the decision boundary. This procedure, however, would only increase the perturbation without changing the median value after reaching  $x + 2g$ . Consequently, the attack requires a lot of queries, converges slower, and returns suboptimal results.

#### 4.4.2 Gradient-Efficient Median Function

To mitigate this problem, we propose to improve the efficiency of standard median function’s gradient by using an efficient median function in its backward pass. Specifically, we define the efficient median function as a “trimmed and weighted average” function. For any input sequence  $x \in [0, 1]^n$ , the efficient median function can be written as

$$\text{efficient-median}(x) := \frac{\sum_{i=1}^n x_i \cdot \omega_i}{\sum_{i=1}^n \omega_i}, \quad (10)$$

where  $\omega \in \mathbb{R}^n$  is the weighting vector.

A useful weighting vector should satisfy two important properties: (1) it proportionally extends the gradient to non-median values; (2) it limits the number of changed values to mitigate the perturbation. We satisfy these two properties through quantile bounding and the absolute deviation to median, which define the weight as

$$\omega_i := (1 - |x_i - \text{median}(x)|) \cdot \mathbb{1}\{x_{(a)} \leq x_i \leq x_{(b)}\}, \quad (11)$$

where  $x_{(a)}, x_{(b)}$  are the  $a$ -th and  $b$ -th quantile of scalar values in  $x$ . We set  $(a, b)$  to  $(0.2, 0.8)$  based on an empirical evaluation in Appendix C. Intuitively, values that deviate more from the median are assigned smaller gradients, and the total number of changed values is limited if all values are close to the median. We note that, however, the above approximation of median function may not be optimal; we leave better-optimized approximations as the future work.

#### 4.4.3 Formalizing the Median Filtering Defenses

Given the above efficient median function, we are ready to formalize the median filtering defense and plug it into the scaling-aware noise sampling in Equation (8). Specifically, we will invoke the modified Algorithm 1 with the original scaling procedure replaced by the median-defended scaling function. However, formulating the median filtering defense is not straightforward because it is originally proposed as a *selective* operation that only modifies vulnerable pixels.

In the following, we will first show how to formulate the selective filtering defense as a *masked pooling layer* with a boolean mask that represents vulnerable pixels. After that, we show a simple strategy to identify these vulnerable pixels.

**Masked Pooling Layer.** We describe the pooling layer as a convolution, as the pooling layer works like a discrete convolution but replaces the linear kernel with some other function [20]. This allows us to represent the defense as

$$\text{defense}(\mathbf{x}) := p(\mathbf{x}) \cdot \text{mask} + \mathbf{x} \cdot (1 - \text{mask}), \quad (12)$$

where  $p$  is the pooling function,  $\text{mask}$  is a boolean mask with 1 denoting vulnerable pixels. The pooling function is given as  $p(\mathbf{x}) := \mathbf{x} \star f$ , where  $\star$  denotes the 2D convolution with reflect padding to keep the same shape, and  $f$  denotes the filter function determined by the defense. In case of the median filtering defense, we set  $f$  to the efficient median function in Equation (10) in the backward pass, and switch to the standard median function in the forward pass.

**Identifying Vulnerable Pixels.** We then explain how to determine the boolean mask in Equation (12). For any fixed scaling algorithm, we can write the scaling function as a matrix multiplication like Equation (1). By setting all entries in the output image  $D \in \mathbb{R}^{p \times q}$  to one and solving for  $S$ , we have

$$S^* = L^+ \times D \times R^+ \in \mathbb{R}^{m \times n}, \quad (13)$$

where  $L^+$  and  $R^+$  are the pseudo-inverse [5] of  $L$  and  $R$ . Conceptually, this recovers the element-wise weight of each pixel in the source image during scaling. That is, every non-zero entry in  $S^*$  indicates a vulnerable pixel in the source image; we thus determine the boolean mask as

$$\text{mask} = \mathbb{1}\{S \neq 0\}, \quad (14)$$

where the indicator function  $\mathbb{1}$  and operator  $\neq$  are all computed in element-wise.

In summary, we have formalized the median filtering defense as a masked pooling layer in Equation (12). This formulation allows us to invoke the scaling-aware HSJ attack in Algorithm 1 with the original scaling function replaced by a composition of the defense and scaling function, written as  $(\text{scale} \circ \text{defense})$ .

## 5 Scaling-aware White-Box Attacks

Finally, we study white-box attacks by exploiting the inconsistency between the  $\ell_2$ -norm robustness claim and the user’s perceptibility expectation. This is useful for transfer-based black-box attacks as well as evaluating the worst-case robustness of ML systems that the user perceives.

Formulating white-box attacks is straightforward, as we only need to view the entire ML pipeline as a sequential model. For example, the objective function of C&W attack [10] becomes

$$\begin{aligned} \min \quad & \|\Delta\|_2 + c \cdot (f \circ \text{scale} \circ \text{defense})(S + \Delta) \\ \text{s.t.} \quad & S + \Delta \in [0, 1]^n, \end{aligned} \quad (15)$$





(a) C&W-Vanilla (scaled  $\ell_2 = 17.44$ )   (b) C&W-Scaling (scaled  $\ell_2 = 5.84$ )   (c) C&W-Medain (scaled  $\ell_2 = 14.4$ )

Figure 6: Adversarial examples from (a) C&W, (b) scaling-aware C&W, and (c) scaling-aware C&W under the median filtering defense. The confidence parameter is set to  $\kappa = 2$ . The original shape is  $224 \times 224$  for (a), and  $672 \times 672$  for (b) and (c). Scaling-aware C&W attack produces less perturbation even under the median defense.

where  $f$  is the loss function quantifying the confidence of ground-truth prediction,  $S$  is the HR source image, and  $\Delta$  is the HR adversarial perturbation. Similarly, the objective function of PGD attack [32] becomes

$$\begin{aligned} \max J((\text{model} \circ \text{scale} \circ \text{defense})(S + \Delta), y) \\ \text{s.t. } \|\Delta\|_2 \leq \epsilon, \end{aligned} \quad (16)$$

where  $J(\cdot)$  is the cross entropy loss,  $y$  is the ground truth label of  $S$ , and  $\epsilon$  is the specified perturbation budget.

**Median Filtering.** From the perspective of a whole ML system pipeline, median filtering can be viewed as a preprocessing defense and circumvented by BPDA [3] in white-box attacks. However, as we find the gradient of our masked pooling layer formulation (used for black-box attacks in Section 4.4) to be useful, we will keep the median filtering formulated as Equation (12) for consistency. We thus do not claim novelty or improvements over BPDA. Adversarial examples produced by scaling-aware C&W attacks are shown in Figure 6.

**Randomized Filtering.** Similarly, the randomized filtering defense can be viewed as a preprocessing defense and circumvented by EoT [4] in white-box attacks. In practice, however, we find this attack inefficient due to a large number of sampling operations and the high resolution of input images. Therefore, we leverage insights of randomized filtering defense to directly calculate its expectation (i.e., the EoT), which reduces the number of samples to zero.

This requires us to examine this defense through its composition with the followed scaling function. Our analysis in Section 3.3 enables us to directly compute its expectation as the area scaling. We thus replace this composition by its expectation in our attack formulation:

$$(\text{scale} \circ \text{defense})(x) := x \star k_{\text{area}}, \quad (17)$$

which reduces the number of samples to zero.

Again, this observation confirms the effectiveness of randomized filtering in Section 3.3. In particular, it is the *interplay* between randomization and the scaling function that makes it effective, not the randomization



itself. This also suggests an interesting insight for EoT: when computing the EoT of one preprocessing defense is hard, one may benefit from viewing this defense together with its followed components (even if such components have no randomization).

**Detection Defenses.** Although we empirically observe that scaling-aware white-box attacks evade all existing detection defenses out of the box, we note that a learning-based detector may still work. In that case, one could adaptively evaluate the detector’s effectiveness using the following approach. Given any detection function  $g$ , we first choose a loss function  $L$  so that  $L(S + \Delta)$  is minimized when the detection  $g(S + \Delta)$  is incorrect. We then add the loss function  $L$  as a regularizer to our objective functions. For instance, Equation (16) would become:

$$\begin{aligned} \max J((\text{model} \circ \text{scale} \circ \text{defense})(S + \Delta), y) - \gamma \cdot L(S + \Delta) \\ \text{s.t. } \|\Delta\|_2 \leq \epsilon, \end{aligned}$$

where  $\gamma$  is the hyper-parameter that controls the weight of the added regularizer. This approach is similar to the attack from Carlini et al. [9] against a learning-based deep-fake detector [25], which also detects the artifacts of deep-fakes in the spectrum domain. We leave the investigation of such attacks to future work.

## 6 Evaluation

Finally, we perform an empirical evaluation of image-scaling defenses and our scaling-aware ML attacks. Our evaluation is designed to answer the following questions<sup>3</sup>.

**Q1: Are scaling defenses still effective when targeting the whole ML system pipeline in a black-box setting?**

We demonstrate that attackers can evade four out of five scaling defenses by targeting the whole ML system in the black-box setting. These defenses include the median filtering [35] and all three detection defenses [29].

**Q2: Can we improve black-box attacks by exploiting the scaling procedure, even under scaling defenses?**

The HSJ attack performs significantly better when it becomes scaling-aware and jointly targets the whole ML pipeline. For the same query budget, scaling-aware HSJ attack generates adversarial examples with less perturbation.

**Q3: Can we improve transfer-based black-box attacks by exploiting the scaling procedure in cloud services?**

We demonstrate that scaling-aware C&W attack generates adversarial examples that transfer to the Tencent Image Analysis API better than a vanilla white-box attack.

**Q4: Can we improve white-box attacks by targeting the whole ML system pipeline? In this setting, how robust are the existing add-on scaling defenses?**

Both C&W and PGD attacks induce a higher drop in the classification accuracy when they become scaling-aware. Further, we verify that only the randomized filtering defense is resistant to scaling-aware white-box attacks.

---

<sup>3</sup>We are ready to release the source code for all evaluations.

## 6.1 Evaluation Setup

**Dataset and Models.** We use the ImageNet dataset [40] with a pre-trained ResNet-50 model [28] for our evaluation. This network accepts input images of size  $224 \times 224$ . From the dataset, we randomly choose 250 images with a scaling ratio above 3 and downscale them to  $672 \times 672$ , which constitute the set of clean source images<sup>4</sup>. We do not consider other standard datasets such as CIFAR10 [30], because they only have low resolution images; downscaling is not part of their processing pipeline.

We use two different pre-trained models. In the black-box setting, we use the model from PyTorch [34], which achieves 76.15% accuracy. In the white-box setting, we use an adversarially trained model [22], which achieves 57.90% accuracy on benign inputs and 35.09% accuracy under a 100-step PGD attack with  $\ell_2$ -norm budget 3. Note that we only choose source images that are correctly classified by the robust model to avoid the artifacts of its slightly lower accuracy.

**Attacks and Setup.** We implement all scaling-aware attacks in PyTorch [34] and ART [33]. For the HopSkipJump [13] attack, we test query budgets in  $\{1000, 2000, \dots, 25000\}$ . For the C&W [10] attack, we set the binary search step to 20 with a maximum of 1,000 iterations. The confidence parameter  $\kappa$  is set to  $\{0, 1, \dots, 10\}$ . For the PGD [32] attack, we set the number of steps to 100 with  $\ell_2$ -norm budget  $\epsilon = \{1, 2, \dots, 20\}$  and step size  $0.1 \times \epsilon$ . We use OpenCV’s linear scaling algorithm to represent vulnerable scaling algorithms. We run all evaluations on an RTX 2080 Ti GPU with 11 GB memory.

**Cloud API.** We deploy transfer-based black-box attacks on Tencent Cloud’s Image Analysis API<sup>5</sup>. It accepts a variety of images and returns Top-5 labels (with probability scores) that best describe the image. We define the ground-truth label as the benign input’s Top-1 label; we only consider benign inputs whose Top-1 score is above 50%. A successful attack should decrease the true label’s score to below 10%. This API still uses OpenCV’s linear scaling without any defense as reported by Xiao et al. [48]. We use the robust model [22] that we attacked in the white-box setting as the surrogate model; attacks on a non-robust model cannot transfer to this API.

**Perceptibility.** We use scaled  $\ell_2$ -norm to quantify the perceptibility of perturbation. This metric is used to fairly compare perturbations between different dimensions [13]. It divides the  $\ell_2$ -norm by the scaling ratio against standard input size  $224 \times 224$ . When referring to the perturbation of adversarial examples, we always compute such perturbation against their benign images in the same dimension. When evaluating a set of images, we report the *median* value of their scaled  $\ell_2$ -norm distances [13].

**Success Attack Rate.** We also report the success rate at various scaled  $\ell_2$ -norm thresholds, given a particular query budget [13]. For instance, under the query budget  $q$  (or confidence requirement  $\kappa$ ), the success rate can be defined as the portion of successful adversarial examples whose scaled  $\ell_2$ -norm perturbation is less than a threshold. This metric shows an attack’s performance under different perturbation constraints.

**Accuracy.** We use the Top-1 accuracy over adversarial inputs to quantify an attack’s strength. All images larger than the network’s input size are filtered (if a defense is applied) and downsampled (with the respective scaling algorithm) before feeding to the network. For randomized filtering, we repeat this procedure 100 times and report as a correct prediction only if all of them are correct.

<sup>4</sup>We only test one scaling ratio due to the space limitation. However, the attacker is free to choose a larger ratio to yield even better results [35, 48].

<sup>5</sup>We have started the responsible disclosure process.

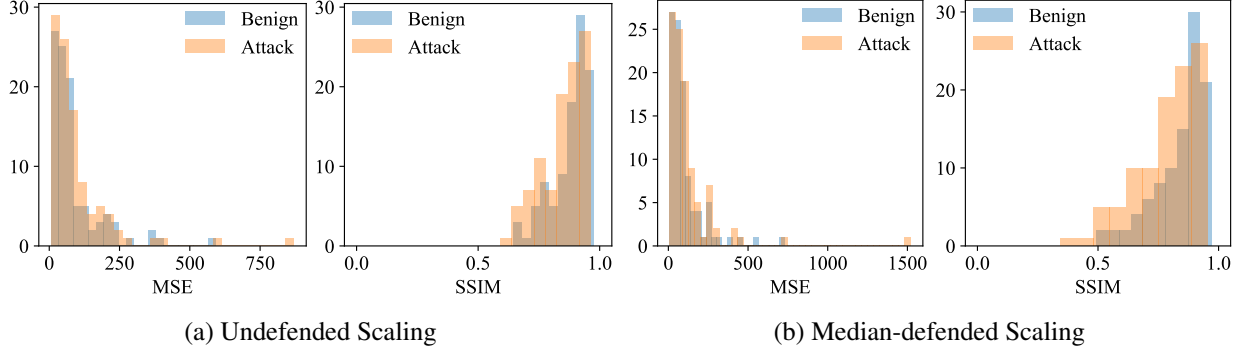


Figure 7: The histogram of distortions as measured by the unscaling defense. There does not exist a reasonable threshold to separate benign images and upstream adversarial examples produced by our scaling-aware HSJA.

## 6.2 Image-Scaling Defenses

In our first experiment, we investigate if existing scaling defenses are still effective when considering the vulnerability of downstream models in the black-box setting. We leverage our scaling-aware HSJ attack with a 5K query budget. This evaluation proceeds in two steps. First, we generate upstream adversarial examples using the scaling-aware HSJ attack with and without the median filtering defense. Second, we run detection defenses on these upstream adversarial examples. The randomized filtering defense will be evaluated in the white-box setup in Section 6.5.

**Evaluation of the Unscaling Defense.** Figure 7 shows the distribution of distortions as measured by the unscaling defense. This defense measures the distortion between the original input image and the upscaled image after applying the downscaling. As we can observe, the distribution is very similar between benign and attack images; there does not exist a reasonable threshold that allows for acceptable false acceptance and rejection rates. We do not report results from the minimum-filtering defense as they show similar observations.

**Evaluation of the Spectrum Defense.** Figure 8 shows the centered spectrum for example benign and attack images. This defense detects the scaling attack by identifying more than one “centered spectrum point” in the spectrum image [29]. As we can observe, the scaling-aware HSJ attack does not exhibit such artifacts.

**Evaluation of the Median Filtering Defense.** We have evaluated this defense along with detection defenses in Figures 7b and 8d. Even under the median filtering defense, the scaling-aware image-scaling attack was able to evade the classifier without significant distortions. A more systematic analysis of the median defense is presented in the following subsection.

**Summary.** The scaling-aware HSJ attack evades four out of five scaling defenses in the black-box threat model where they claim robustness. It shows that different vulnerabilities in an ML system can exacerbate each other, thereby breaking defenses that are developed in isolation of the ML system.

## 6.3 Scaling-aware Black-Box Attacks

In our second experiment, we examine if black-box attacks can exploit the vulnerability in scaling algorithms to reduce their perturbation and queries. This reduction would motivate an attacker to target the entire ML system pipeline instead of a standalone model.

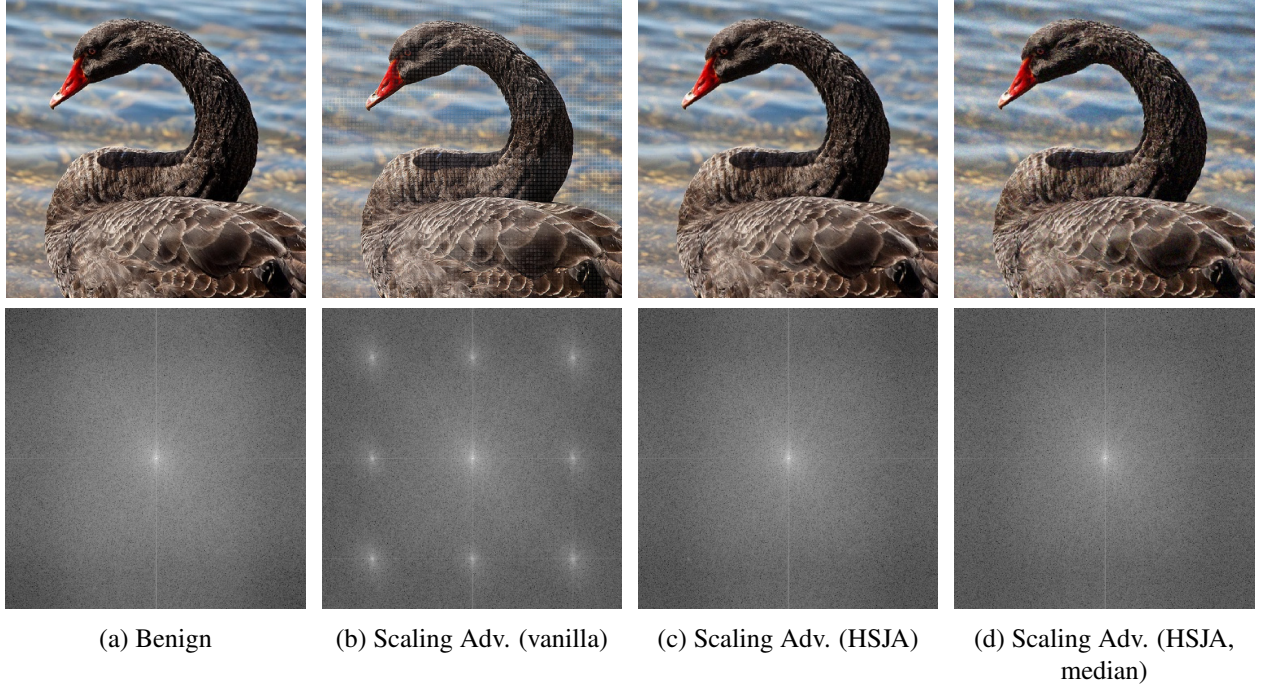


Figure 8: Centered spectrum images of (a) benign, (b) standard scaling attack, (c) scaling-aware HSJA, and (d) scaling-aware HSJA under the median filtering defense. Our scaling-aware HSJ attacks do not exhibit artifacts like (b).

This evaluation proceeds in two steps. For each query budget  $q \in \{1000, 2000, \dots, 25000\}$ , we use the vanilla HSJA to generate a set of LR adversarial examples  $\mathcal{L}(q)$ , and use the scaling-aware HSJA to generate a set of HR adversarial examples  $\mathcal{H}(q)$ . After that, we compare the perturbation between  $\mathcal{L}(q)$  and  $\mathcal{H}(q)$ .

**Evaluation of the Perturbation.** Figure 9a shows the median perturbation generated by attacks with given query budgets. For undefended scaling, scaling-aware HSJA can reduce the perturbation by a large margin. Note that the generated adversarial examples still evade all detection defenses. For median-defended scaling, scaling-aware HSJA converges faster to a better solution than vanilla HSJA.

**Evaluation of the Query Budget.** Figure 9b shows the success rate of vanilla and scaling-aware HSJAs with given perturbation budgets. For undefended scaling, scaling-aware HSJA boosts the success rate by a large margin. For median-defended scaling, scaling-aware HSJA still achieves higher success rates with the same query budget. It is clear how the dashed lines of scaling-aware HSJA are way above the dotted lines of vanilla HSJA, even with 5K fewer query budgets.

**Ablation Study.** Figure 10 shows the performance of scaling-aware attacks when our proposed novel techniques (for incorporating scaling) are disabled. Figure 10a clearly shows that blindly targeting the entire pipeline (w/o SNS) cannot exploit the vulnerability in scaling. Figure 10b shows that our proposed efficient median function can significantly improve the convergence, otherwise the “scaling-aware” attack is almost impractical. These results confirm the effectiveness of our proposed novel techniques. Interestingly, Figure 10b also suggests the median filter as a potential preprocessing defense against black-box attacks (where BPDA [3] does not apply) on the ML model, and our proposed efficient median as a potential evasion. We did not evaluate this conjecture because it is out of the scope of this paper.

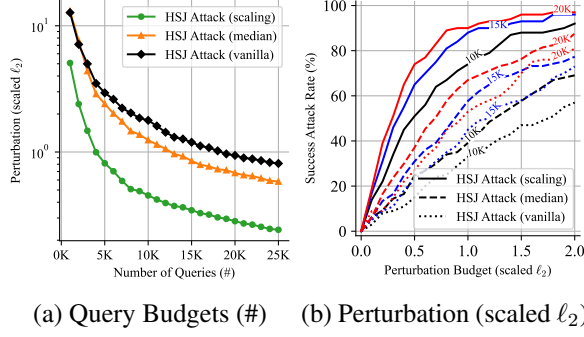


Figure 9: Comparison of scaling-aware HSJ attacks against no defense (scaling), against the median defense (median), and the vanilla HSJ attack under different constraints. The scaling-aware HSJ attack outperforms the vanilla attack by a large margin even under the median filtering defense.

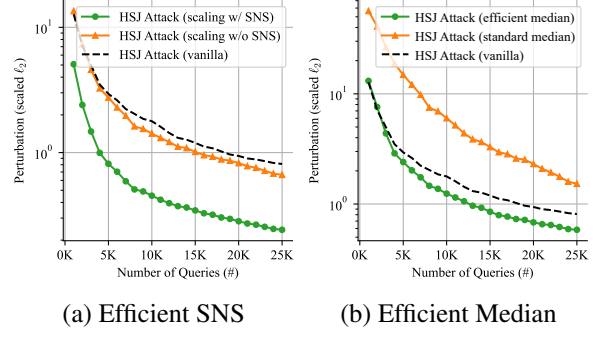


Figure 10: Ablation study of our (a) efficient SNS and (b) efficient median. SNS makes it possible to exploit scaling, otherwise the performance is similar to a vanilla attack. Efficient median enables the attack to converge faster under the median defense, otherwise the performance is even worse than a vanilla attack.

**Joint vs. Sequential Attacks.** Figure 11 compares the performance of our joint attack and the alternative sequential attack (all based on HSJA). The sequential attack injects adversarial examples from vanilla HSJA to their HR source images. Figure 11a shows that jointly attacking the pipeline uses the query budget more efficiently; the 5K joint attack even beats the 20K sequential attack. Figure 11b shows that the sequential attack is suboptimal under the median defense; it becomes worse when the target adversarial example was obtained with more queries (thus, more sensitive to the imprecise results from image-scaling attacks).

**Summary.** The scaling-aware HSJ attack outperforms the vanilla attack by a large margin (even under median filtering defense). It shows that the vulnerability in scaling can exacerbate the vulnerability in ML models, thereby improving ML attacks. This observation also suggests that the vulnerability in scaling could compromise the user-perceived robustness of ML systems, as we discussed in Section 4.

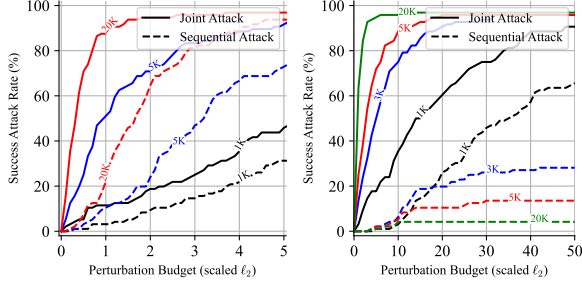
## 6.4 Scaling-aware Transfer-based Attacks

In our third experiment, we examine if transfer-based black-box attacks can exploit the vulnerability in scaling to improve their transferability while reducing the perturbation. In particular, we test Tencent Cloud’s Image Analysis API by attacking a surrogate model using our scaling-aware C&W attack, as described in Section 5.

The evaluation proceeds in two steps. For each confidence  $\kappa \in \{0, 1, \dots, 10\}$ , we generate adversarial examples on the surrogate model. After that, we send such examples to the Image Analysis API and measure the success rate. Similar to the setting of query-based attacks in Section 6.3, we perform this procedure using the vanilla and scaling-aware C&W attacks to obtain the set of LR and HR examples  $\mathcal{L}(\kappa)$  and  $\mathcal{H}(\kappa)$ , respectively. Note that we examine the transferability against median filtering defense in the following Section 6.5, as we could not find a Cloud API that implements this defense.

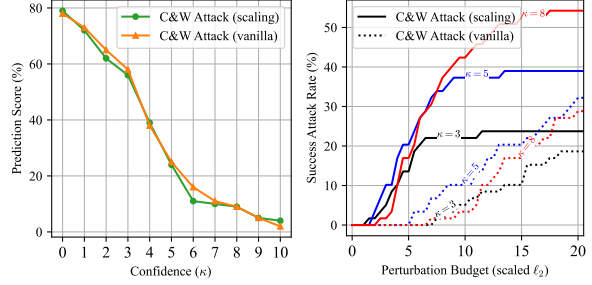
**Evaluation of the Cloud API.** Figure 12 shows the transferability of vanilla and scaling-aware C&W attacks on Tencent Cloud API. Figure 12a shows that both attacks are producing equally-confident adversarial examples (from the API’s perspective) if given the same confidence parameter. This observation confirms





(a) Scaling & No Defense (b) Scaling & Median Def.

Figure 11: Comparison of the joint and sequential attacks on the entire pipeline. Our joint attack is significantly better than the sequential one. Interestingly, the sequential attack in (b) becomes worse when the target adversarial example was obtained with more queries, as opposed to the joint attack.



(a) Confidence ( $\kappa$ ) (b) Perturbation (scaled  $\ell_2$ )

Figure 12: Compare the transferability of vanilla and scaling-aware C&W attacks on the Tencent Cloud API. The prediction score is returned by the API and indicates how confident it predicts the input as its ground-truth label.

that the scaling-aware C&W attack does not misuse the confidence parameter to overclaim improvements in the following evaluation. Thus, as we can observe from Figure 12b, the scaling-aware C&W attack achieves significantly higher success rates than vanilla C&W under perturbation constraints. Notably, the scaling-aware attack even outperforms high-confident vanilla attacks with only  $\kappa = 3$ .

**Summary.** The scaling-aware transfer-based attacks can significantly outperform their vanilla attacks. It shows that the vulnerability of scaling algorithms in an ML system can exacerbate the vulnerability in ML models. Again, this observation suggests that scaling vulnerabilities could compromise the user-expected robustness of downstream ML models.

## 6.5 Worst-case Robustness Evaluation

Finally, we evaluate the robustness of the entire ML system pipeline under threats from both the scaling procedure and the ML model. For this purpose, we protect the scaling algorithms with median or randomized filtering defense, and protect the ML model with adversarial training.

We use scaling-aware C&W and PGD attacks in Section 5 to evaluate the robustness under the confidence and perturbation constraint, respectively. Similar to the setting in Section 6.4, we generate two sets of adversarial examples using the vanilla and scaling-aware attacks, respectively.

Figure 13 shows the performance of scaling-aware white-box attacks when attacking the entire ML system pipeline. Overall, scaling-aware attacks are able to gain incentives under no scaling defense or the median filtering defense. In Figure 13a, the scaling-aware C&W attack was able to achieve the same confidence with lower perturbation. In Figure 13b, the scaling-aware PGD attack was able to decrease more accuracy with the same perturbation budget.

The only exception is the randomized filtering defense in Figure 13b, which successfully protects the ML system’s robustness against threats from the scaling procedure. We show that scaling algorithms adopting uniform kernels or dynamic kernel widths [35] are robust as well in Appendix D.

**Summary.** An attacker can compromise the ML system’s robustness by jointly exploiting the vulnerability in scaling procedure and ML models, especially when defenses are developed in isolation of the entire ML system pipeline. It suggests defenders consider the interplay between vulnerabilities in ML systems.

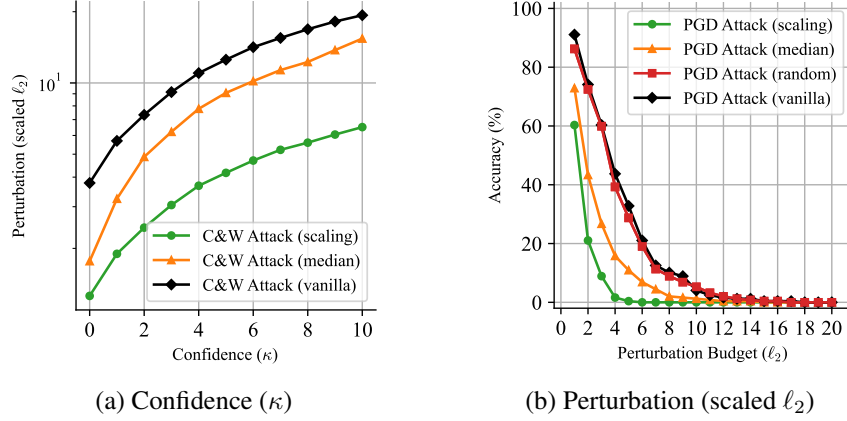


Figure 13: Compare the performance of scaling-aware white-box attacks under different constraints and prevention scaling defenses. Only the randomized filtering defense is robust.

## 7 Conclusion

This paper investigates the interplay between the vulnerabilities of the image scaling procedure and ML models in the black-box setting. We propose a series of novel techniques to make an attack aware of the scaling procedure and effectively leverage the weakness of scaling algorithms and defenses. By targeting the entire ML system, an attacker can improve the performance of ML attacks while evading most existing defenses against the scaling attack. Our results exhibit that an attacker can produce stronger adversarial examples with less perturbation and lower query budgets if targeting the entire ML system. The purpose of this work is to raise the concern of threats that jointly exploit different vulnerabilities in the ML system. We believe that further work is necessary to identify and mitigate other threats that jointly target different components in the ML system.



## References

- [1] *2016 IEEE Conference on Computer Vision and Pattern Recognition, CVPR 2016, Las Vegas, NV, USA, June 27-30, 2016*. IEEE Computer Society, 2016.
- [2] *6th International Conference on Learning Representations, ICLR 2018, Vancouver, BC, Canada, April 30 - May 3, 2018, Conference Track Proceedings*. OpenReview.net, 2018.
- [3] Anish Athalye, Nicholas Carlini, and David A. Wagner. Obfuscated gradients give a false sense of security: Circumventing defenses to adversarial examples. In Dy and Krause [21], pages 274–283.
- [4] Anish Athalye, Logan Engstrom, Andrew Ilyas, and Kevin Kwok. Synthesizing robust adversarial examples. In Dy and Krause [21], pages 284–293.
- [5] Adi Ben-Israel and Thomas NE Greville. *Generalized inverses: theory and applications*, volume 15. Springer Science & Business Media, 2003.
- [6] Battista Biggio, Iginio Corona, Davide Maiorca, Blaine Nelson, Nedim Šrndić, Pavel Laskov, Giorgio Giacinto, and Fabio Roli. Evasion attacks against machine learning at test time. In *Joint European conference on machine learning and knowledge discovery in databases*, pages 387–402. Springer, 2013.
- [7] Wieland Brendel, Jonas Rauber, and Matthias Bethge. Decision-based adversarial attacks: Reliable attacks against black-box machine learning models. In *6th International Conference on Learning Representations, ICLR 2018, Vancouver, BC, Canada, April 30 - May 3, 2018, Conference Track Proceedings*. OpenReview.net, 2018.
- [8] Nicholas Carlini, Anish Athalye, Nicolas Papernot, Wieland Brendel, Jonas Rauber, Dimitris Tsipras, Ian Goodfellow, Aleksander Madry, and Alexey Kurakin. On evaluating adversarial robustness, 2019.
- [9] Nicholas Carlini and Hany Farid. Evading deepfake-image detectors with white- and black-box attacks. In *2020 IEEE/CVF Conference on Computer Vision and Pattern Recognition, CVPR Workshops 2020, Seattle, WA, USA, June 14-19, 2020*, pages 2804–2813. IEEE, 2020.
- [10] Nicholas Carlini and David A. Wagner. Towards evaluating the robustness of neural networks. In *2017 IEEE Symposium on Security and Privacy, SP 2017, San Jose, CA, USA, May 22-26, 2017*, pages 39–57. IEEE Computer Society, 2017.
- [11] Varun Chandrasekaran, Chuhan Gao, Brian Tang, Kassem Fawaz, Somesh Jha, and Suman Banerjee. Face-off: Adversarial face obfuscation. *Proc. Priv. Enhancing Technol.*, 2021(2):369–390, 2021.
- [12] Varun Chandrasekaran, Hengrui Jia, Anvith Thudi, Adelin Travers, Mohammad Yaghini, and Nicolas Papernot. Sok: Machine learning governance, 2021.
- [13] Jianbo Chen, Michael I. Jordan, and Martin J. Wainwright. Hopskipjumpattack: A query-efficient decision-based attack. In *2020 IEEE Symposium on Security and Privacy, SP 2020, San Francisco, CA, USA, May 18-21, 2020*, pages 1277–1294. IEEE, 2020.
- [14] Yufei Chen, Chao Shen, Cong Wang, Qixue Xiao, Kang Li, and Yu Chen. Scaling camouflage: Content disguising attack against computer vision applications. IEEE, 2020.

- [15] Minhao Cheng, Thong Le, Pin-Yu Chen, Huan Zhang, Jinfeng Yi, and Cho-Jui Hsieh. Query-efficient hard-label black-box attack: An optimization-based approach. In *7th International Conference on Learning Representations, ICLR 2019, New Orleans, LA, USA, May 6-9, 2019*. OpenReview.net, 2019.
- [16] Minhao Cheng, Simranjit Singh, Patrick H. Chen, Pin-Yu Chen, Sijia Liu, and Cho-Jui Hsieh. Sign-opt: A query-efficient hard-label adversarial attack. In *8th International Conference on Learning Representations, ICLR 2020, Addis Ababa, Ethiopia, April 26-30, 2020*. OpenReview.net, 2020.
- [17] Valeriia Cherepanova, Micah Goldblum, Harrison Foley, Shiyuan Duan, John P. Dickerson, Gavin Taylor, and Tom Goldstein. Lowkey: Leveraging adversarial attacks to protect social media users from facial recognition. In *9th International Conference on Learning Representations, ICLR 2021, Virtual Event, Austria, May 3-7, 2021*. OpenReview.net, 2021.
- [18] Jeremy M. Cohen, Elan Rosenfeld, and J. Zico Kolter. Certified adversarial robustness via randomized smoothing. In Kamalika Chaudhuri and Ruslan Salakhutdinov, editors, *Proceedings of the 36th International Conference on Machine Learning, ICML 2019, 9-15 June 2019, Long Beach, California, USA*, volume 97 of *Proceedings of Machine Learning Research*, pages 1310–1320. PMLR, 2019.
- [19] Vincent Dumoulin and Francesco Visin. A guide to convolution arithmetic for deep learning. *CoRR*, abs/1603.07285:6–8, 2016.
- [20] Vincent Dumoulin and Francesco Visin. A guide to convolution arithmetic for deep learning. *CoRR*, abs/1603.07285:6–8, 2016.
- [21] Jennifer G. Dy and Andreas Krause, editors. *Proceedings of the 35th International Conference on Machine Learning, ICML 2018, Stockholmsmässan, Stockholm, Sweden, July 10-15, 2018*, volume 80 of *Proceedings of Machine Learning Research*. PMLR, 2018.
- [22] Logan Engstrom, Andrew Ilyas, Hadi Salman, Shibani Santurkar, and Dimitris Tsipras. Robustness (python library), 2019.
- [23] Ivan Evtimov, Weidong Cui, Ece Kamar, Emre Kiciman, Tadayoshi Kohno, and Jerry Li. Security and machine learning in the real world. *arXiv preprint arXiv:2007.07205*, 2020.
- [24] Ivan Evtimov, Pascal Sturmfels, and Tadayoshi Kohno. Foggysight: A scheme for facial lookup privacy. *CoRR*, abs/2012.08588, 2020.
- [25] Joel Frank, Thorsten Eisenhofer, Lea Schönherr, Asja Fischer, Dorothea Kolossa, and Thorsten Holz. Leveraging frequency analysis for deep fake image recognition. In *Proceedings of the 37th International Conference on Machine Learning, ICML 2020, 13-18 July 2020, Virtual Event*, volume 119 of *Proceedings of Machine Learning Research*, pages 3247–3258. PMLR, 2020.
- [26] Chuan Guo, Jacob R. Gardner, Yurong You, Andrew Gordon Wilson, and Kilian Q. Weinberger. Simple black-box adversarial attacks. In Kamalika Chaudhuri and Ruslan Salakhutdinov, editors, *Proceedings of the 36th International Conference on Machine Learning, ICML 2019, 9-15 June 2019, Long Beach, California, USA*, volume 97 of *Proceedings of Machine Learning Research*, pages 2484–2493. PMLR, 2019.
- [27] Chuan Guo, Mayank Rana, Moustapha Cissé, and Laurens van der Maaten. Countering adversarial images using input transformations. In *6th International Conference on Learning Representations, ICLR 2018, Vancouver, BC, Canada, April 30 - May 3, 2018, Conference Track Proceedings [2]*.

- [28] Kaiming He, Xiangyu Zhang, Shaoqing Ren, and Jian Sun. Deep residual learning for image recognition. In *2016 IEEE Conference on Computer Vision and Pattern Recognition, CVPR 2016, Las Vegas, NV, USA, June 27-30, 2016* [1], pages 770–778.
- [29] Bedeuro Kim, Alsharif Abuadbba, Yansong Gao, Yifeng Zheng, Muhammad Ejaz Ahmed, Surya Nepal, and Hyoungshick Kim. Decamouflage: A framework to detect image-scaling attacks on CNN. In *51st Annual IEEE/IFIP International Conference on Dependable Systems and Networks, DSN 2021, Taipei, Taiwan, June 21-24, 2021*, pages 63–74. IEEE, 2021.
- [30] Alex Krizhevsky, Geoffrey Hinton, et al. Learning multiple layers of features from tiny images. 2009.
- [31] Yujia Liu, Seyed-Mohsen Moosavi-Dezfooli, and Pascal Frossard. A geometry-inspired decision-based attack. In *2019 IEEE/CVF International Conference on Computer Vision, ICCV 2019, Seoul, Korea (South), October 27 - November 2, 2019*, pages 4889–4897. IEEE, 2019.
- [32] Aleksander Madry, Aleksandar Makelov, Ludwig Schmidt, Dimitris Tsipras, and Adrian Vladu. Towards deep learning models resistant to adversarial attacks. In *6th International Conference on Learning Representations, ICLR 2018, Vancouver, BC, Canada, April 30 - May 3, 2018, Conference Track Proceedings* [2].
- [33] Maria-Irina Nicolae, Mathieu Sinn, Minh Ngoc Tran, Beat Buesser, Ambrish Rawat, Martin Wistuba, Valentina Zantedeschi, Nathalie Baracaldo, Bryant Chen, Heiko Ludwig, Ian Molloy, and Ben Edwards. Adversarial robustness toolbox v1.6.0. *CoRR*, 1807.01069, 2018.
- [34] Adam Paszke, Sam Gross, Francisco Massa, Adam Lerer, James Bradbury, Gregory Chanan, Trevor Killeen, Zeming Lin, Natalia Gimelshein, Luca Antiga, Alban Desmaison, Andreas Kopf, Edward Yang, Zachary DeVito, Martin Raison, Alykhan Tejani, Sasank Chilamkurthy, Benoit Steiner, Lu Fang, Junjie Bai, and Soumith Chintala. Pytorch: An imperative style, high-performance deep learning library. In H. Wallach, H. Larochelle, A. Beygelzimer, F. d'Alché-Buc, E. Fox, and R. Garnett, editors, *Advances in Neural Information Processing Systems 32*, pages 8024–8035. Curran Associates, Inc., 2019.
- [35] Erwin Quiring, David Klein, Daniel Arp, Martin Johns, and Konrad Rieck. Adversarial preprocessing: Understanding and preventing image-scaling attacks in machine learning. In *29th USENIX Security Symposium, USENIX Security 2020, August 12-14, 2020*, pages 1363–1380, 2020.
- [36] Erwin Quiring and Konrad Rieck. Backdooring and poisoning neural networks with image-scaling attacks. In *2020 IEEE Security and Privacy Workshops, SP Workshops, San Francisco, CA, USA, May 21, 2020*, pages 41–47. IEEE, 2020.
- [37] Ali Rahmati, Seyed-Mohsen Moosavi-Dezfooli, Pascal Frossard, and Huaiyu Dai. Geoda: A geometric framework for black-box adversarial attacks. In *2020 IEEE/CVF Conference on Computer Vision and Pattern Recognition, CVPR 2020, Seattle, WA, USA, June 13-19, 2020*, pages 8443–8452. Computer Vision Foundation / IEEE, 2020.
- [38] Joseph Redmon, Santosh Kumar Divvala, Ross B. Girshick, and Ali Farhadi. You only look once: Unified, real-time object detection. In *2016 IEEE Conference on Computer Vision and Pattern Recognition, CVPR 2016, Las Vegas, NV, USA, June 27-30, 2016* [1], pages 779–788.

- [39] Shaoqing Ren, Kaiming He, Ross B. Girshick, and Jian Sun. Faster R-CNN: towards real-time object detection with region proposal networks. In Corinna Cortes, Neil D. Lawrence, Daniel D. Lee, Masashi Sugiyama, and Roman Garnett, editors, *Advances in Neural Information Processing Systems 28: Annual Conference on Neural Information Processing Systems 2015, December 7-12, 2015, Montreal, Quebec, Canada*, pages 91–99, 2015.
- [40] Olga Russakovsky, Jia Deng, Hao Su, Jonathan Krause, Sanjeev Satheesh, Sean Ma, Zhiheng Huang, Andrej Karpathy, Aditya Khosla, Michael S. Bernstein, Alexander C. Berg, and Fei-Fei Li. Imagenet large scale visual recognition challenge. *Int. J. Comput. Vis.*, 115(3):211–252, 2015.
- [41] Shawn Shan, Emily Wenger, Jiayun Zhang, Huiying Li, Haitao Zheng, and Ben Y. Zhao. Fawkes: Protecting privacy against unauthorized deep learning models. In Srdjan Capkun and Franziska Roesner, editors, *29th USENIX Security Symposium, USENIX Security 2020, August 12-14, 2020*, pages 1589–1604. USENIX Association, 2020.
- [42] Ilia Shumailov, Zakhar Shumaylov, Dmitry Kazhdan, Yiren Zhao, Nicolas Papernot, Murat A. Erdogdu, and Ross Anderson. Manipulating sgd with data ordering attacks. 2021.
- [43] Ilia Shumailov, Yiren Zhao, Daniel Bates, Nicolas Papernot, Robert Mullins, and Ross Anderson. Sponge examples: Energy-latency attacks on neural networks. In *6th IEEE European Symposium on Security and Privacy (EuroS&P)*, 2021.
- [44] Christian Szegedy, Sergey Ioffe, Vincent Vanhoucke, and Alexander A. Alemi. Inception-v4, inception-resnet and the impact of residual connections on learning. In Satinder P. Singh and Shaul Markovitch, editors, *Proceedings of the Thirty-First AAAI Conference on Artificial Intelligence, February 4-9, 2017, San Francisco, California, USA*, pages 4278–4284. AAAI Press, 2017.
- [45] Christian Szegedy, Vincent Vanhoucke, Sergey Ioffe, Jonathon Shlens, and Zbigniew Wojna. Rethinking the inception architecture for computer vision. In *2016 IEEE Conference on Computer Vision and Pattern Recognition, CVPR 2016, Las Vegas, NV, USA, June 27-30, 2016* [1], pages 2818–2826.
- [46] Christian Szegedy, Wojciech Zaremba, Ilya Sutskever, Joan Bruna, Dumitru Erhan, Ian J. Goodfellow, and Rob Fergus. Intriguing properties of neural networks. *CoRR*, abs/1312.6199, 2013.
- [47] Adelin Travers, Lorna Licollari, Guanghan Wang, Varun Chandrasekaran, Adam Dziedzic, David Lie, and Nicolas Papernot. On the exploitability of audio machine learning pipelines to surreptitious adversarial examples. *arXiv preprint arXiv:2108.02010*, 2021.
- [48] Qixue Xiao, Yufei Chen, Chao Shen, Yu Chen, and Kang Li. Seeing is not believing: Camouflage attacks on image scaling algorithms. In Nadia Heninger and Patrick Traynor, editors, *28th USENIX Security Symposium, USENIX Security 2019, Santa Clara, CA, USA, August 14-16, 2019*, pages 443–460. USENIX Association, 2019.

## A Analyze Randomized Filtering Defense

In the following arguments, we show that the randomized filtering defense indeed meets the robustness requirement.

Without loss of generality, we study randomized filtering over a  $3 \times 3$  window  $w$  in the source image  $S$  and an arbitrary convolution kernel  $k$ . We also pad the input properly so the window  $w$  is always surrounded by other pixels. Since both the scaling and filtering functions can be written as a convolution, we restate the defended scaling  $D = (\text{scale} \circ \text{defense})(S)$  over a window  $w$  with output pixel  $d_{2,2}$  as

$$\begin{aligned} d_{2,2} &= w \star f_{\text{rnd}} \star k \\ &= \begin{bmatrix} w_{1,1} & w_{1,2} & w_{1,3} \\ w_{2,1} & w_{2,2} & w_{2,3} \\ w_{3,1} & w_{3,2} & w_{3,3} \end{bmatrix} \star f_{\text{rnd}} \star \begin{bmatrix} k_{1,1} & k_{1,2} & k_{1,3} \\ k_{2,1} & k_{2,2} & k_{2,3} \\ k_{3,1} & k_{3,2} & k_{3,3} \end{bmatrix}, \end{aligned}$$

where the randomized filter  $f_{\text{rnd}}$  randomly picks a pixel from the  $3 \times 3$  window  $w$  with probability  $1/9$ .

We study the central pixel  $w_{2,2}$  and its weight  $w'_{2,2}$  during this defended scaling. First, the randomized filtering slides a  $3 \times 3$  window around each pixel  $w_{i,j}$  and randomly changes its value to  $w_{2,2}$  with a probability  $\Pr[w_{i,j} \leftarrow w_{2,2}] = 1/9$ . Second, the scaling algorithm gives the weight  $k_{i,j}$  to each pixel  $w_{i,j}$ . Since the pixel  $w_{i,j}$  could hold the value of  $w_{2,2}$ , the overall weight of  $w_{2,2}$  can be described as  $\Pr[w'_{2,2} \leftarrow k_{i,j}] = 1/9$ . Thus, we can write the expected value of the weight  $w'_{2,2}$  as

$$\mathbb{E}_{f \sim \mathcal{F}}[w'_{2,2}] = \sum_{1 \leq i,j \leq 3} \frac{1}{9} \cdot k_{i,j} = \frac{1}{9}, \quad (18)$$

where  $\mathcal{F}$  is the filter space determined by  $f_{\text{rnd}}$  and we have assumed a normalized scaling kernel  $k$ . This shows that the pixel  $w_{2,2}$  is given a uniform weight in expectation. Extending to other pixels, we have:

$$\mathbb{E}_{\text{defense} \sim \mathcal{D}}[(\text{scale} \circ \text{defense})(S)] = S \star k_{\text{area}}, \quad (19)$$

where  $\mathcal{D}$  is the space of defense functions chosen by the randomized filtering defense and  $k_{\text{area}}$  is the uniform area scaling kernel defined in Section 2.3.3.

## B Exploiting Vulnerabilities Sequentially

In Section 4, we have shown how to *jointly* exploit vulnerabilities in upstream scaling and downstream classifier. However, we note that it is also possible to *sequentially* exploit these two vulnerabilities. For example, the attacker can deploy the conventional black-box attacks on the downstream model, and leverage the image-scaling attack to hide the adversarial example within its original clean image. This requires solving Equation (3), where  $T$  is the standard adversarial example generated by a black-box attack on the downstream model.

However, we note that the sequential attack is suboptimal. This attack only finds an HR image whose downsampled version is close enough to the given LR adversarial example; it cannot guarantee that the obtained HR image is still adversarial after downsampling. As black-box adversarial examples are typically near the decision boundary, the final solution may still lie in the correct label's decision area even if it is close enough to the given adversarial example. This problem is more severe when it is hard to precisely invert the median filtering defense. Our evaluation results in Figure 11 confirms this argument. We thus focus on the more practical joint attack, which directly optimizes to attack the entire ML system.

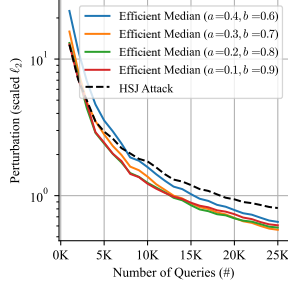


Figure 14: The performance of our scaling-aware HSJA (with efficient median) under the median filtering defense and the vanilla HSJA. We show different quantile bounds in Equation (11).

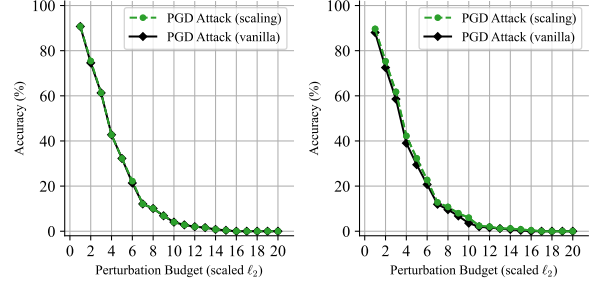


Figure 15: Compare the performance of vanilla and scaling-aware PGD attacks on scaling algorithms that are robust by design. This verifies the robustness of such scaling algorithms.

Finally, we conjecture that the sequential attack only works when the given target image can induce a misclassification with high probability, such as an image from another class (like the standard image-scaling attack) or an adversarial example generated by the C&W attack with high confidence.

## C Approximation of Median’s Gradient

In Section 4.4, we approximate the median function by “trimmed and weighted average” to provide a useful gradient for black-box attacks. To this end, we introduce the weight with quantile bounding, as defined in Equation (11). In this section, we provide empirical evaluations of different choices of the quantile position  $a$  and  $b$ .

As we can observe from Figure 14, more constrained bounds could result in suboptimal performance, such as  $(0.4, 0.6)$  and  $(0.3, 0.7)$ . In contrast, we observe that relaxed bounds could obtain better performance, such as  $(0.2, 0.8)$  and  $(0.1, 0.9)$ . We finally choose  $(0.2, 0.8)$  as it obtains better performance when given lower query budgets (5K) and higher budgets (25K).

## D Evaluate Robust Scaling Algorithms

Recall that Quiring et al. [35] have identified a few scaling algorithms that are robust against the scaling attack (see Section 2.3.3). We also evaluate their robustness against the scaling-aware image-scaling attack. In Figure 15, we report the evaluation of scaling algorithms that adopt uniform kernels (CV Area) or dynamic kernel widths (PIL Linear). As evident from the plots, scaling-aware PGD attacks cannot exploit these scaling algorithms to improve the vanilla one. This verifies the robustness of known-robust scaling algorithms in a setting where the attacker jointly targets the whole ML system pipeline.

## E Black-box Adversarial Examples by HSJA

Figure 16 shows more black-box adversarial examples from our scaling-aware HSJ attack. scaling-aware HSJA is able to produce less perturbation than the vanilla HSJA for a given query budget. The same observation holds for median-defended scaling after 200 model queries.



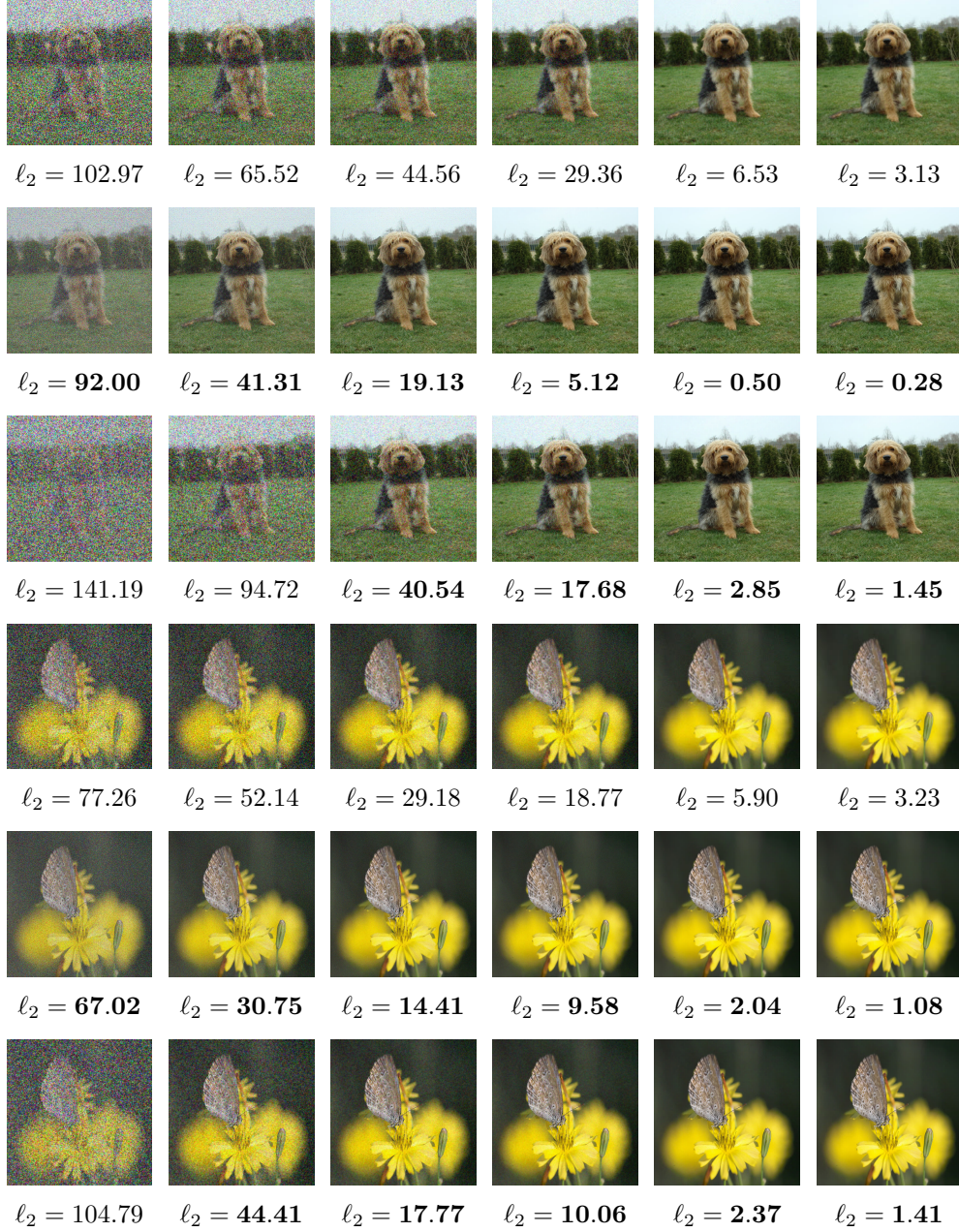


Figure 16: Adversarial examples in the black-box setting. 1st–3rd (4th–6th) rows: examples generated by HSJA, scaling-aware HSJA, and scaling-aware HSJA under the median filtering defense. 1st–6th columns: examples at 100, 200, 500, 1K, 5K, 10K model queries. Perturbations: the scaled  $\ell_2$ -norm distance to the original image, numbers in bold font denote obtaining less perturbation than the vanilla HopSkipJump attack. The shape of above images from HSJA and scaling-aware HSJA is  $224 \times 224$  and  $672 \times 672$ , respectively.